

Short-time dynamics of finite-size mean-field systems

Celia Anteneodo

*Departamento de Física, PUC-Rio and National Institute
of Science and Technology for Complex Systems,*

*Rua Marquês de São Vicente 225, Gávea,
CEP 22453-900 RJ, Rio de Janeiro, Brazil*

Ezequiel E. Ferrero and Sergio A. Cannas

*Facultad de Matemática, Astronomía y Física,
Universidad Nacional de Córdoba and Instituto
de Física Enrique Gaviola (IFEG-CONICET),
Ciudad Universitaria, 5000 Córdoba, Argentina*

Abstract

We study the short-time dynamics of a mean-field model with non-conserved order parameter (Curie-Weiss with Glauber dynamics) by solving the associated Fokker-Planck equation. We obtain closed-form expressions for the first moments of the order parameter, near to both the critical and spinodal points, starting from different initial conditions. This allows us to confirm the validity of the short-time dynamical scaling hypothesis in both cases. Although the procedure is illustrated for a particular mean-field model, our results can be straightforwardly extended to generic models with a single order parameter.

PACS numbers: 64.60.Ht, 05.10.Gg, 64.60.My, 64.60.an

Keywords: Mean-field models, Short-time dynamics, Fokker-Planck equation

I. INTRODUCTION

Universal scaling behavior appears to be an ubiquitous property of critical dynamic systems. While initially believed to hold only in the long time limit, it was realized during the last decade that the dynamical scaling hypothesis can be extended to the short-time limit [1]. This is accomplished by assuming that, close to the critical point, the n th moment of the order parameter obeys the homogeneity relation

$$m^{(n)}(t, \tau, L, m_0) = b^{-n\beta/\nu} m^{(n)}(b^{-z}t, b^{1/\nu}\tau, L/b, b^\mu m_0), \quad (1)$$

where t is time, τ is the reduced temperature $\tau = (T_c - T)/T_c$, L is the linear system size, m_0 is the initial value of the order parameter and b is a spatial rescaling parameter. μ is a universal exponent that describes the short-time behavior, while β , ν , and z are the usual critical exponents. When $m_0 \ll 1$ we recover the usual dynamic scaling relation, from which a power law relaxation at the critical point (for instance, in the magnetization $n = 1$) $m(t) \sim t^{-\beta/\nu z}$ when $L \gg 1$ and $t \gg 1$ follows. This is the critical slowing down.

On the other hand, the short-time dynamics (STD) scaling properties of the system depend on the initial preparation, i.e., on the scaling field m_0 . Setting $b = t^{1/z}$, from Eq. (1) one obtains for small (but non-null) values of $t^{\mu/z} m_0$ in the large L limit

$$m(t, \tau, m_0) \sim m_0 t^\theta F(t^{1/\nu z} \tau), \quad \theta = \frac{\mu - \beta/\nu}{z}. \quad (2)$$

Hence, at the critical point $\tau = 0$ an initial increase of the magnetization $m \sim m_0 t^\theta$ is observed. For the second moment $n = 2$ the dependency on m_0 can be neglected when $m_0 \ll 1$. Since $m^{(2)} \sim N^{-1} = L^{-d}$ in the large L limit (d is the spatial dimension), one obtains at the critical point

$$m^{(2)}(t) \sim N^{-1} t^{d/z - 2\beta/z\nu}. \quad (3)$$

The short-time universal scaling behavior has been verified in a large variety of critical systems both by renormalization group (RG) calculations [1, 2] and Monte Carlo (MC) numerical simulations [3–5]. The hypothesis also applies when the system starts in the completely ordered state, i.e., $m_0 = 1$. In this case it is assumed that the homogeneity relation

$$m^{(n)}(t, \tau, L) = b^{-n\beta/\nu} m^{(n)}(b^{-z}t, b^{1/\nu}\tau, L/b) \quad (4)$$

holds even for short (macroscopic) time scales. Hence, in the large L limit we have

$$m(t) = t^{-\beta/\nu z} G(t^{1/\nu z} \tau), \quad (5)$$

and taking the derivative of $\log m$,

$$\left. \frac{\partial \log m(t, \tau)}{\partial \tau} \right|_{\tau=0} \sim t^{1/\nu z}. \quad (6)$$

While the scaling hypothesis starting from the disordered state is supported both by numerical simulations and RG, its validity for an initial ordered state relies up to now only on numerical simulations.

Recently, numerical simulations have shown that the short-time scaling hypothesis (1) holds not only close to a critical point, but also close to spinodal points in systems exhibiting a first-order phase transition, both for mean-field and short-range interactions models [6]. This is particularly interesting, because it suggests the existence of some kind of diverging correlation length associated to a spinodal point. Since the proper concept of spinodal in short-range interactions systems is still a matter of debate (see Ref. [6] and references therein), a deeper understanding of the microscopic mechanisms behind the observed short time scaling could shed some light on this problem. One way of achieving this goal is to look for exact solutions of particular models. A first step in that direction is to analyze mean-field (i.e., infinite-range interactions) models, for which the concept of spinodal is well defined [6]. That is the objective of the present work: we analyze the exact STD behavior of far from equilibrium mean-field systems with non-conserved order parameter.

Non-equilibrium phenomena in physics and other fields are commonly studied through Fokker-Planck equations (FPEs). In particular, non-equilibrium dynamical aspects of phase transitions can be analyzed by means of the FPE associated to the master equation describing the microscopic dynamics [7–9]. In fact, this tool was proved to be useful in the description of the relaxation of metastable states [7], finite-size effects [10] or the impact of fluctuations in control parameters [11], and have been considered for mean-field spin models [7, 12] and coupled oscillators [10], amongst many others.

As soon as the degrees of freedom of the system can be reduced to a few relevant ones, a low-dimensional FPE can be found. Although this description is suitable for properties that do not depend on the details of the dynamics, or for mean-field kinetics, many conclusions are expected to hold in more general instances.

For a single order parameter m , the FPE for its probability $P = P(m, t|m_0, 0)$ is

$$\partial_t P = [-\partial_m D_1(m) + \partial_{mm} D_2(m)] P \equiv L_{FP}(m)P, \quad (7)$$

where the drift and diffusion coefficients are determined by the Hamiltonian and the particular dynamics (e.g., Glauber or Metropolis).

Following this stochastic approach, here we study the scaling of the short-time relaxational dynamics in the vicinity of critical and spinodal points. In first approximation, the drift $D_1(m)$ ($= -dV/dm$) is generically linear in the vicinity of a critical point and quadratic in the spinodal, following the quadratic and cubic behavior of the drift potential V , respectively. Meanwhile, typically in various models, the noise intensity $D_2(m)$ scales as $\epsilon \sim 1/N$ [7, 10]. Therefore, although we will present the STD for a particular spin model, our results can be straightforwardly extended to more general mean-field ones.

II. FORMAL FPE SOLUTION AND MOMENT EXPANSIONS

The formal solution of the FPE (7), for the initial condition $P(m, 0|m_0, 0) = \delta(m - m_0)$, is [13]

$$P(m, t|m_0, 0) = e^{tL_{FP}(m)} \delta(m - m_0).$$

The average of an arbitrary quantity $Q(m)$ can be derived directly from the FPE, by means of the adjoint Fokker-Plank operator $L_{FP}^\dagger(m) \equiv D_1 \partial_m + D_2 \partial_{mm}$, as follows

$$\begin{aligned} \langle Q \rangle(m_0, t) &= \int Q(m) P(m, t|m_0, 0) dm = \int Q(m) e^{tL_{FP}(m)} \delta(m - m_0) dm \\ &= \int \delta(m - m_0) e^{tL_{FP}^\dagger(m)} Q(m) dm = e^{tL_{FP}^\dagger(m_0)} Q(m_0) = \\ &= \sum_{k \geq 0} [L_{FP}^\dagger(m_0)]^k Q(m_0) t^k / k!. \end{aligned} \quad (8)$$

Therefore, the first two moments of the order parameter are

$$\begin{aligned} \langle m \rangle &= m_0 + D_1 t + \frac{1}{2} [D_1 D_1' + D_2 D_1''] t^2 + \dots, \\ \langle m^2 \rangle &= \langle m \rangle^2 + 2D_2 t + [2D_2 D_1' + D_1 D_2' + D_2 D_2''] t^2 + \dots, \end{aligned} \quad (9)$$

where D_1 , D_2 and their derivatives are evaluated in m_0 . Notice that if D_1 and D_2 are not state-dependent, the expansion up to first order is exact.

Alternatively, evolution equations for moments can be obtained by integration of Eq. (7), after multiplying each member of the equation by the quantity to be averaged, that is

$$\frac{d\langle m^n \rangle}{dt} = n \langle m^{n-1} D_1(m) \rangle + n(n-1) \langle m^{n-2} D_2(m) \rangle. \quad (10)$$

For $n = 1$ we have

$$\frac{d\langle m \rangle}{dt} = \langle D_1(m) \rangle. \quad (11)$$

Eqs.(10) lead in general to a hierarchy of coupled equations for the moments. Only for a few special cases (D_1 and D_2 polynomials in m of degree smaller or equal than one and two respectively) these equations decouple. Otherwise, one has to rely on approximated methods to solve their dynamics.

III. PARADIGMATIC MEAN-FIELD MODEL

Let us exhibit our STD analysis for the paradigmatic system of N fully connected Ising spins (Curie-Weiss model), subject to a magnetic field H , ruled by the mean-field Hamiltonian

$$\mathcal{H} = -\frac{J}{2N} M^2 - HM. \quad (12)$$

Since the Hamiltonian depends only on the total magnetization M , the master equation for this model can be written in closed form for M [7, 12]. In the large N limit, when the magnetization per spin $m = M/N$ can be taken as a continuous variable, an expansion of the master equation up to first order in the perturbative parameter $\epsilon = 1/N$ leads for the Glauber dynamics to a FP equation (7) with [12]

$$\begin{aligned} D_1(m) &= -m + \tanh[m'] - \epsilon \beta J m \operatorname{sech}^2[m'], \\ D_2(m) &= \epsilon (1 - m \tanh[m']), \end{aligned} \quad (13)$$

where we have defined $m' = \beta(Jm + H)$, with $\beta = 1/(k_B T)$.

In the next sections we derive asymptotic solutions of the FPE with these coefficients, both close to the critical point ($H = 0$ and $T \approx T_c = J/k_B$) and to spinodal points for $T < T_c$. Analytical results are compared against Monte Carlo simulation ones using Glauber algorithm. Time was adimensionalized with the characteristic time t_0 of the transition rate

$w = t_0^{-1}(1 + \exp(\beta\Delta\mathcal{H}))^{-1}$. The unit of time in theoretical expressions corresponds to one MC step in simulations. We also performed several checks using Metropolis algorithm. The outcomes were indistinguishable from the Glauber ones, except for a trivial time rescaling factor 2 close to the critical point, as expected [7].

IV. STD NEAR THE CRITICAL POINT

In the vicinity of the critical point (at $T \simeq T_c = J/k_B \equiv 1$ and $H = 0$), the coefficients (13) can be approximated for small m (i.e., $\beta J|m| \ll 1$) respectively by

$$\begin{aligned} D_1(m) &= -\omega(\lambda, \epsilon) m - \kappa(\lambda, \epsilon) m^3 + \mathcal{O}(m^5), \\ D_2(m) &= \epsilon ([1 - (1 - \lambda)m^2] + \mathcal{O}(m^4)), \end{aligned} \quad (14)$$

where $\omega(\lambda, \epsilon) \equiv \lambda + \epsilon(1 - \lambda)$ and $\kappa(\lambda, \epsilon) \equiv (\frac{1}{3} - \epsilon)(1 - \lambda)^3$, with $\lambda \equiv 1 - T_c/T$.

Within the domain of validity of these approximations $(1 - \lambda)m^2 \ll 1$ and therefore $D_2 \simeq \epsilon$. Concerning D_1 , its linear term dominates, that is,

$$D_1(m) \simeq -\omega(\lambda, \epsilon) m, \quad (15)$$

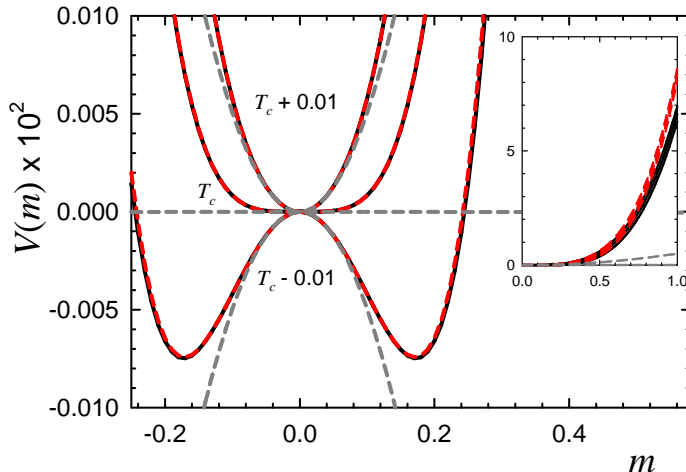


FIG. 1: (Color online) Potential $V(m)$, for different values of T in the vicinity of T_c , indicated in the figure. It was obtained (unless an arbitrary additive constant) from the integration of D_1 in Eqs. (13) (black full lines), (14) (red dashed lines) and (15) (gray dashed lines). Inset: zoom of the region close to $m = 1$.

if

$$|\omega| \gg \kappa m^2. \quad (16)$$

This implies a parabolic approximation of the drift potential $V(m) = -\int D_1(m)dm$, whose shape is plotted in Fig. 1 for different values of $T \simeq T_c$, found from the integration of D_1 in Eq. (13) and of the linearized expression(15), for comparison. For $\omega > 0$, one has a confining quadratic potential, while for $\omega < 0$ the parabolic potential is inverted, with an unstable point at $m = 0$.

A. Ornstein-Uhlenbeck approximation

Now, for linear D_1 and constant D_2 , the exact solution of Eq. (7) reads [13]

$$P(m, t|m_0, 0) = \frac{1}{\sqrt{2\pi\sigma^2(t)}} \exp\left(-\frac{[m - m_0 \exp(-\omega t)]^2}{2\sigma^2(t)}\right), \quad (17)$$

where $\sigma^2(t) = \epsilon[1 - \exp(-2\omega t)]/\omega$. This solution applies for $\omega > 0$ (Ornstein-Uhlenbeck (OU) process) as well as for $\omega < 0$, and is valid as long as the probability distribution remains strongly peaked so that the inequality (16) holds for any value of m with non-negligible probability.

Performing the average with Eq. (17) gives

$$\langle m \rangle = m_0 \exp(-\omega t). \quad (18)$$

Therefore, for $\omega > (<)0$, that is $T/T_c > (<)1 - 1/N$, the average magnetization decays (grows) exponentially, with characteristic time $|\omega|^{-1}$. Then, for time scales $t \ll |\omega|^{-1}$, it remains $\langle m \rangle \sim m_0$. Since in the large N limit $\omega \sim \lambda$, then the magnetization scales as $\langle m \rangle = m_0 F(\lambda t)$. This is consistent with Eq. (2), provided that $\theta = 0$ and $\nu z = 1$, in agreement with the mean-field exponents $\nu = 1/2$ and $z = 2$. The same exponents are displayed by the Gaussian model [1]. For higher-order moments $m^{(n)} \equiv \langle (m - \langle m \rangle)^n \rangle$ with even $n \geq 2$, one has

$$m^{(n)} = \frac{\Gamma(\frac{n+1}{2})}{\sqrt{\pi}} [2\epsilon \omega^{-1} (1 - \exp[-2\omega t])]^{\frac{n}{2}}. \quad (19)$$

Then, for short times $t \ll 1/|\omega|$,

$$m^{(n)} \sim [\epsilon t]^{n/2}. \quad (20)$$

Hence, $m^{(2)} \sim t/N$, consistently with Eq. (3) ($\beta = 1/2$), provided that we choose $d = 4$, the upper critical dimension.

The characteristic time scale for STD behavior is then $t \ll \tau_{STD}$ with

$$\tau_{STD} \approx \frac{1}{|\lambda + \epsilon|} = \frac{N}{|1 + N\lambda|}. \quad (21)$$

If $|\lambda N| \gg 1$ we have $\tau_{STD} \sim 1/|\lambda| \ll N$, while for $|\lambda N| \ll 1$ we have $\tau_{STD} \sim N$.

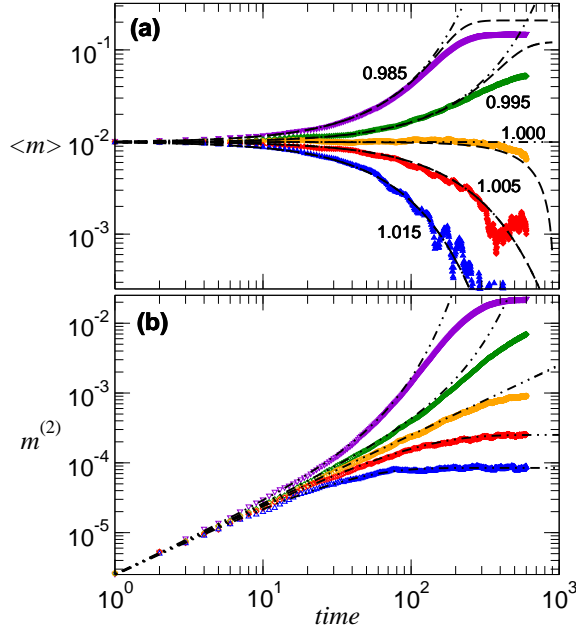


FIG. 2: (Color online) First and second moments of the order parameter as a function of time t , for $m_0 = 0.01$ and different values of $T \simeq T_c = 1$. (a) Magnetization: black dot-dashed lines correspond to Eq. (18) and black dashed ones to Eq. (22). (b) Second moment: black dot-dashed lines correspond to Eq. (19). Numerical simulations using Glauber dynamics were performed for $N = 8 \times 10^5$ (color symbols).

Fig. 2 displays the comparison between numerical simulations and the approximate OU solutions Eqs. (18)-(19), for $N = 8 \times 10^5$, $m_0 = 0.01$ and different values of $T \simeq T_c$, such that $|\lambda N| \gg 1$. The OU approximation gives an excellent agreement for time scales up to $t \sim \tau_{STD}$ ($\tau_{STD} \sim 100$ for the present parameter values). Averages were taken over 1000 independent MC runs. The main differences between the theoretical and numerical results appear for $T < T_c$ and $t > \tau_{STD}$, where finite-size effects shift the equilibrium value of both the average magnetization and its variance.

Fig. 2 also shows the performance of Eq. (22), which reproduces the simulation results for longer times than Eq. (18), predicting the transient steady state. The lower saturation level observed in simulation outcomes for $T < T_c$ is due to the presence of fluctuations

that drive some trajectories to the equilibrium state with negative magnetization, while the deterministic equation rules the stabilization at the level of the local minimum. Also notice that this discrepancy decreases as T departs from the critical value because of the consequent increase of the potential barrier height, which makes such events less probable. For $T > T_c$, the system evolves quickly towards the vicinity of the equilibrium state and the saturation level of the second moment is very close to the value given by the (bimodal) steady state distribution $P(m) \propto \exp(-V(m)/\epsilon)$. In any case, finite-size higher order corrections can be neglected as far as the STD behavior is concerned.

B. Quartic approximation of the drift potential

When (16) does not apply, one can not discard the cubic contribution to D_1 . For such case we show in Appendix A that the inclusion of the cubic correction in the drift coefficient Eq. (14) leads for $\epsilon \ll 1$ to

$$\langle m \rangle = \frac{m_0 e^{-\omega t}}{\sqrt{1 + m_0^2 \kappa (1 - e^{-2\omega t}) / \omega}}. \quad (22)$$

This solution is exact in the thermodynamic limit $\epsilon \rightarrow 0$, as can be verified by direct integration of the deterministic version of Eq. (11) [7], i.e.,

$$\frac{d\langle m \rangle}{dt} = D_1(\langle m \rangle). \quad (23)$$

Notice that the expansion of Eq. (22) up to first order in m_0 reproduces Eq. (18). The case $\omega = 0$ ($T = T_c$), can also be drawn from Eq. (22) by taking the limit $\omega \rightarrow 0$, yielding

$$\langle m \rangle = \frac{m_0}{\sqrt{1 + 2m_0^2 \kappa t}}. \quad (24)$$

In Appendix A we additionally show that finite-size corrections do not change the STD scaling of $\langle m \rangle$. For the second moment we obtain

$$m^{(2)} \equiv \langle m^2 \rangle - \langle m \rangle^2 = 2\epsilon t \frac{(1+z)(1+2z+2z^2)}{(1+2z)^3} + \mathcal{O}(\epsilon^2, \epsilon\omega), \quad (25)$$

where $z \equiv \kappa m_0^2 t$. Notice that up to a typical time scale $1/(2\kappa m_0^2)$, the approximation $m^{(2)} \simeq 2\epsilon t$ holds. For $\kappa m_0^2 t \gg 1$, a crossover to a second linear (hence normal diffusive) regime but with a different diffusion constant is predicted, namely $m^{(2)} \simeq \epsilon t/2$, although it typically falls beyond the STD region.

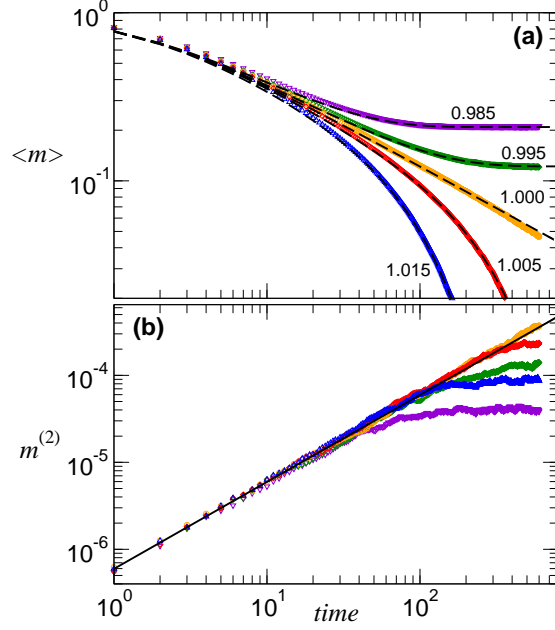


FIG. 3: (Color online) First and second moments as a function of time t for $m_0 = 1$ and different values of $T \simeq T_c = 1$. (a) Magnetization: dashed lines correspond to theoretical results given by Eq. (22). (b) Second moment: the full black line represents $2D_2(m_0 = 1)t$. Numerical simulations using Glauber dynamics were performed for $N = 8 \times 10^5$ (color symbols).

C. Other initial conditions

To investigate the scaling behavior for other initial conditions, we analyzed the STD behavior when $m_0 = 1$. As can be seen in the inset of Fig. 1, the cubic approximation still holds close to $m = 1$. Hence, the thermodynamic-limit expression (22) is expected to apply too, as verified in Fig. 3a. In comparison with the initial condition of Fig. 2, here trajectories get more trapped around the positive minimum, hence the agreement with deterministic Eq. (22) is still better. For finite systems, the intensity of the fluctuations is state dependent following Eq. (13). Therefore, the finite-size corrections derived by assuming $D_2 \simeq \epsilon$ do not hold. However, for very short times one still expects $m^{(2)} \sim 2D_2(m_0)t$, according to Eq. (9), as in fact verified in numerical simulations illustrated in Fig. 3. From Eq. (22) we have that $m(t) \sim t^{-1/2}(1 - \lambda t)$ for $t \ll 1/|\lambda|$, in agreement with Eq. (5). The excellent accord between Eq. (22) and numerical simulation outcomes displayed in Fig. 3 when $|\lambda N| \gg 1$ confirms our previous assumptions. Numerical simulations for other values of N also verify the above scaling. For $T > T_c$ the equilibrium (final steady state) values of both mean and

variance are quickly approached as in Fig.2. However, when $T < T_c$, we see from Fig.3b that all the curves lie below the critical curve, at variance with the behavior observed when $m_0 \ll 1$ (compare with Fig.2b). This is because when $m_0 = 1$ almost all the trajectories get trapped in the positive minimum. Thus, the variance stabilizes in a value corresponding to the fluctuations in a single potential minimum. At long enough times, both minima in a finite size system get equally populated and therefore the equilibrium value of $m^{(2)}$ will be higher. However, the time scales needed to observe this effect fall outside the STD regime. On the contrary, when $m_0 \ll 1$, a relatively large number of trajectories cross the barrier between minima and $m^{(2)}$ approaches the equilibrium value (which is larger than the steady one), even at very short times, as can be verified by comparing the numerical plateaux in Fig.2b with the equilibrium value

$$m_{eq}^{(2)} = \frac{\int_{-1}^1 m^2 e^{-\frac{V(m)}{\epsilon}} dm}{\int_{-1}^1 e^{-\frac{V(m)}{\epsilon}} dm}. \quad (26)$$

V. STD NEAR THE SPINODAL

When $T < T_c$ the model has a line of first-order transitions at $H = 0$ and metastable stationary solutions for a range of values of H . Without loss of generality we will restrict hereafter to the metastable solutions with positive magnetization, that is, those analytic continuations of the equilibrium magnetization from positive to negative values of H . Defining $h \equiv \beta H$, the metastable state exists as long as $h > h_{SP}$, where the spinodal field is given by

$$h_{SP} = -\beta J m_{SP} + \frac{1}{2} \ln \frac{1 + m_{SP}}{1 - m_{SP}}$$

$$m_{SP} = \sqrt{1 - \frac{1}{\beta J}}.$$

where m_{SP} is the magnetization at the spinodal point [6].

Suppose now that we start the system evolution from the completely ordered state $m_0 = 1$ with $T < T_c$ and $h > h_{SP}$ and let us define $\Delta m \equiv m - m_{SP}$ and $\Delta h \equiv h - h_{SP}$. Considering Δm as an order parameter, numerical simulations using Metropolis dynamics [6] showed that close enough to the spinodal point ($|\Delta h| \ll 1$) its moments obey the scaling form (4) with $\tau = \Delta h / h_{SP}$. For temperatures far enough from T_c the spinodal magnetization m_{SP} is close to one and we can expand D_1 and D_2 in powers of Δh and Δm . Moreover, close to the spinodal we can neglect [12] the finite-size correction of D_1 . Then, from Eqs. (13) one

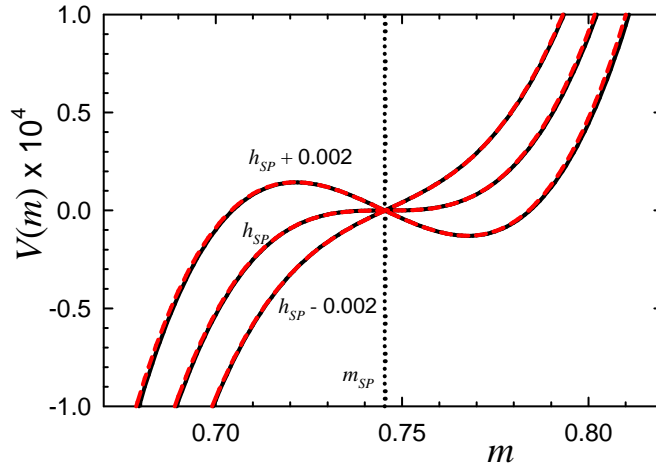


FIG. 4: (Color online) Potential $V(m)$, for different values of h in the vicinity of h_{SP} , indicated in the figure for $T = 4/9$. It was computed (unless an arbitrary additive constant) from the integration of D_1 in Eq. (13) (red full lines) and (27) (black dashed lines).

has at first order in Δh and second order in Δm :

$$\begin{aligned}
 D_1(m) &\simeq \frac{\Delta h}{\beta J} - 2m_{SP}\Delta m\Delta h - \beta J m_{SP}(\Delta m)^2, \\
 D_2(m) &\simeq \epsilon \left(\frac{1}{\beta J} - 2m_{SP}\Delta m + (\beta J - 2)(\Delta m)^2 \right. \\
 &\quad \left. - \frac{m_{SP}}{\beta J}\Delta h + \left(2 - \frac{3}{\beta J}\right)\Delta m\Delta h \right). \quad (27)
 \end{aligned}$$

In Fig. 4 we plot the shape of $V(m)$ for different values of h in the vicinity of h_{SP} , obtained both from integration of D_1 in Eq. (13) and of the approximate quadratic polynomial (27), for comparison.

The moments of Δm can be calculated by means of Eq. (8), namely

$$\langle (\Delta m)^n \rangle = \sum_{k \geq 0} [D_1 \partial_x + D_2 \partial_{xx}]^k x^n t^k / k!, \quad (28)$$

where we have defined $x \equiv m_0 - m_{SP}$.

For $n = 1$ we can neglect in a first approximation the diffusion term, that is, at least for short times we can disregard finite-size effects. Then, from Eq. (28) using $D_1 = -A(x^2 + 2A\alpha x - \alpha)$, with $\alpha = \Delta h / (\beta J A)$ and $A \equiv \beta J m_{SP}$ one has (see Appendix B)

$$\langle \Delta m \rangle = \sqrt{\gamma} \frac{u + \tanh(\sqrt{\gamma} At)}{1 + u \tanh(\sqrt{\gamma} At)} - A\alpha, \quad (29)$$

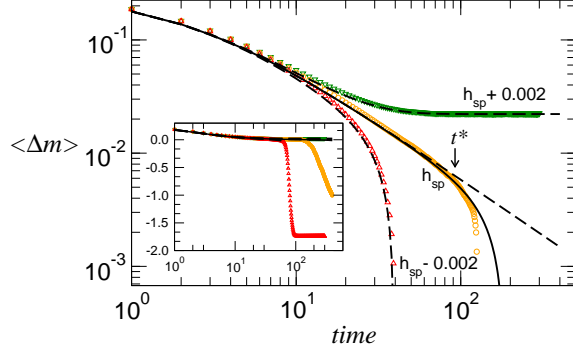


FIG. 5: (Color online) Mean magnetization as a function of time t , for $m_0 = 1$, $T = 4/9$ and different values of h . Black dashed lines correspond to the prediction given by Eqs. (29)-(31). The full black line corresponds to Eq. (B4). The inset is the same plot in linear-log scales. Numerical simulations were performed for $N = 8 \times 10^5$ (color symbols).

where $u = (x + A\alpha)/\sqrt{\gamma}$ and $\gamma = \alpha + A^2\alpha^2$. For $\alpha < 0$ (hence $\gamma < 0$), Eq. (29) becomes

$$\langle \Delta m \rangle = \sqrt{|\gamma|} \frac{u - \tan(\sqrt{|\gamma|}At)}{1 + u \tan(\sqrt{|\gamma|}At)} - A\alpha. \quad (30)$$

Alternatively, Eqs. (29)-(30) can be obtained by integrating Eq. (23), and are in good agreement with numerical simulations, as illustrated in Fig. (5). One observes the following asymptotic behaviors:

(i) For $|h| < |h_{SP}|$ ($\alpha > 0$), a constant level is reached. In fact, since the potential presents a local minimum, the plateau occurs at a level associated to that minimum. This is in accord with numerical simulations (Fig. 5), notice that the local minimum of the potential is at $m \simeq 0.768$, then $\Delta m = m - m_{SP} \simeq 0.023$, in agreement with the observed level.

(ii) For $|h| > |h_{SP}|$: ($\alpha < 0$), Eq. (30) yields a rapid decay towards zero attained at finite t . This is because the potential is tilted towards the absolute minimum (without local minimum).

In the limit $\alpha \rightarrow 0$, from Eq. (29) it follows

$$\langle \Delta m \rangle = \frac{x}{1 + Axt}. \quad (31)$$

Hence, at the spinodal point one has $\langle \Delta m(t) \rangle \sim t^{-1}$ for $t \gg 1/Ax$, consistently with Eq. (5) with $\beta = 1/2$ and $\nu z = 1/2$, in agreement with previous numerical results [6]. This behavior corresponds to the relaxation towards the saddle point $m = m_{SP}$. While in an infinite system such point is an stationary state, finite-size fluctuations destabilize it, with the subsequent

exponential relaxation towards the equilibrium value $\Delta m \gtrsim -1 - h_{SP}$ at longer times, as depicted in Fig. 5. Finite-size corrections to Eq. (31), that we compute for $\Delta h = 0$, can be obtained by including the diffusion term in Eq. (28). When $\Delta h = 0$, following Eq. (27), we have $D_2(x) \simeq \epsilon(ax^2 + bx + c)$, with $a = \beta J - 2$, $b = -2m_{SP}$, $c = 1/\beta J$ and $D_1 = -Ax^2$. In Appendix B we obtain Eq. (B4), furnishing $\langle \Delta m \rangle$ corrected at first order in ϵ , that for $t \gg 1/Ax$ leads to

$$\langle \Delta m \rangle \sim \frac{1}{At} \left[1 - \frac{\epsilon c A^2}{10} t^3 + \mathcal{O}(\epsilon t^2, \epsilon^2) \right]. \quad (32)$$

Hence, finite-size effects will become relevant only when $t \sim t^*$, with

$$t^* = \left(\frac{10\beta J}{\epsilon A^2} \right)^{1/3} = \left(\frac{10 N}{-\lambda} \right)^{1/3}, \quad (33)$$

in agreement with the scaling proposed in Ref. [6]: $t^* \propto N^{z/d_c}$, with $z = 2$ and $d_c = 6$.

Finally, let us consider the second moment. In Appendix B we obtain Eq. (B6), that gives the ϵ -correction to $\langle (\Delta m)^2 \rangle$. It allows to compute $\Delta m^{(2)} = \langle (\Delta m)^2 \rangle - (\langle \Delta m \rangle)^2$, Eq. (B7), that at short times $t \ll 1/Ax$ leads to

$$\Delta m^{(2)} \sim 2\epsilon(ax^2 + bx + c)t \simeq 2D(x)t, \quad (34)$$

in accord with Eq. (9).

Meanwhile, for $t \gg 1/Ax$, Eq. (B6) behaves as

$$\langle (\Delta m)^2 \rangle \sim \frac{1}{(At)^2} \left[1 + \frac{\epsilon c A^2}{5} t^3 + \mathcal{O}(\epsilon t^2, \epsilon^2) \right]. \quad (35)$$

Hence from Eqs. (32) and (35) one gets

$$\Delta m^{(2)} \sim \frac{2\epsilon c t}{5}. \quad (36)$$

Notice that in this regime, the prefactor of t given by Eq. (36) is generically different from that obtained in the very short-time regime following Eq. (34). Fig. (6) illustrates this cross-over for different values of m_0 and fixed temperature. The prefactor at small times, $2D_2(m_0)$ varies with m_0 (panel a), while at intermediate times $1/Ax \ll t < t^*$ the prefactor becomes $\frac{2}{5}\epsilon c = \frac{2\epsilon}{5\beta J}$ independently of m_0 , which is evident in the linear scale (panel b).

In any case the behavior $\Delta m^{(2)} \sim \epsilon t$ up to $t \sim t^*$ is consistent with the STD scaling hypothesis for the set of mean-field exponents $z\nu = 2$, $\beta = 1/2$, $d_c = 6$ and in agreement with numerical outcomes [6].

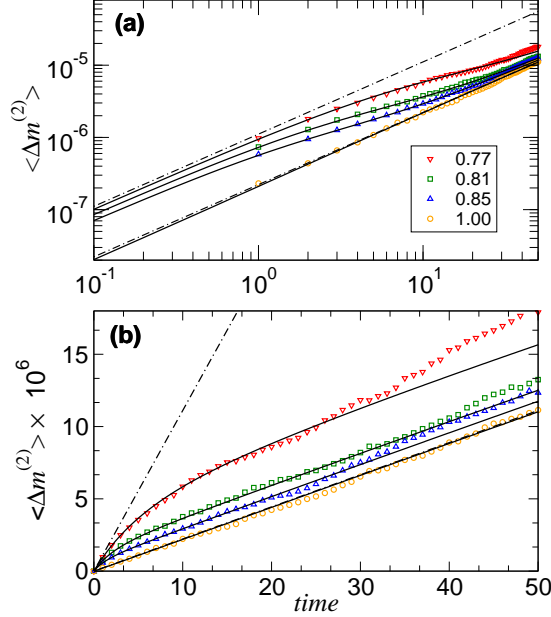


FIG. 6: (Color online) Second moment of the order parameter as a function of time t , for $T = 4/9$, $h = h_{SP}$ and different values of m_0 (with $m_{SP} < m_0 < 1$). Panels (a) and (b) display the same data in logarithmic and linear scales, respectively. Black full lines correspond to the prediction given by Eq. (B6). Symbols correspond to MC numerical simulations for $N = 8 \times 10^5$. The dash-dotted lines correspond to $2D_2(m_{sp})t$ (upper line) and $2/5 c \epsilon t$ (lower line).

VI. FINAL COMMENTS

We studied the short-time dynamical behavior of finite-size mean-field models (infinite-range interactions) with non conserved order parameter dynamics. By solving the associated Fokker-Plank equation we obtained closed expressions for the first moments of the order parameter, in the vicinity of both the critical and spinodal points. This allowed us to confirm the STD scaling hypothesis in both situations, as well as to determine the dynamical ranges of its validity. In particular, we confirmed analytically its validity when the system starts from an ordered state. Moreover, we found that a diffusion-like scaling behavior of the second moment appears for any initial value of the order parameter, but the associated diffusion coefficient presents a crossover between two different values, for short and intermediate times within the STD regime.

We found in general that the scaling behavior of the first moment is mainly determined by the shape of the potential $V(m) = -\int D_1(m)dm$ and therefore by the equilibrium

generalized free energy $f(m, T, H)$, which has the same extrema structure as [7] $V(m)$. The scaling behavior of higher moments, on the other hand, has its origin on the Gaussian nature of finite-size fluctuations close to the singular points. Although our results were obtained for a particular model, it is worth to stress that the above facts are characteristic of mean-field systems, since they depend only on the shape of $V(m)$ and on the proportionality $D_2 \propto 1/N$. This makes the analysis quite general and independent of the particular mean-field model.

Acknowledgments: The authors would like to thank T. S. Grigera and E. S. Loscar for sharing with us their simulation codes for Metropolis dynamics, as well as for useful discussions. This work was supported by CNPq and Faperj (Brazil), CONICET, Universidad Nacional de Córdoba, and ANPCyT/FONCyT (Argentina).

Appendix A: Quartic potential approximation near the critical point

To investigate the effect of including the cubic correction in the drift coefficient Eq. (14), we evaluate the particular setting of Eq. (8)

$$\langle m^n \rangle = \sum_{k \geq 0} [(-\omega m_0 - \kappa m_0^3) \partial_{m_0} + \epsilon \partial_{m_0 m_0}]^k \frac{m_0^n t^k}{k!}. \quad (\text{A1})$$

In the limit $|\lambda N| \gg 1$, we can neglect in a first approximation the diffusion term and compute

$$\langle m \rangle \approx \sum_{k \geq 0} [(-\omega m_0 - \kappa m_0^3) \partial_{m_0}]^k \frac{m_0 t^k}{k!}.$$

By iterating the operator k times and identifying the general form of the coefficients of t^k , with the aid of symbolic manipulation programs, we obtain

$$\begin{aligned} \langle m \rangle &\approx m_0 \sum_{k, j \geq 0} \frac{(-\omega t)^k}{k!} \binom{2j}{j} \left(-\frac{m_0^2 \kappa}{4\omega}\right)^j \sum_{i=0}^j \binom{j}{i} (-1)^i (2i+1)^k \\ &= m_0 e^{-\omega t} \sum_{j \geq 0} \binom{2j}{j} \left(-\frac{m_0^2 \kappa}{4\omega}\right)^j (1 - e^{-2\omega t})^j \\ &= \frac{m_0 e^{-\omega t}}{\sqrt{1 + m_0^2 \kappa (1 - e^{-2\omega t}) / \omega}}, \end{aligned} \quad (\text{A2})$$

that coincides with the exact deterministic solution (22).

Fluctuations can be neglected as long as $\kappa, \omega \sim O(\epsilon^0)$. However, while 3κ remains of order one (except for extreme temperatures), typically $\omega \sim \lambda + \epsilon \ll 1$. Then, a finite-size correction can be included by keeping only the terms of order ϵ and ω in each coefficient of t^k in Eq. (A1). This procedure yields the correction term,

$$\begin{aligned} C_1(\epsilon) &= -\epsilon\kappa m_0 t^2 \sum_{k \geq 0} \binom{2k}{k} (2k^2 + 6k + 3) (-z/2)^k \\ &= -\epsilon\kappa m_0 t^2 \frac{3 + 4z + 2z^2}{(1 + 2z)^{5/2}}, \end{aligned}$$

where $z \equiv \kappa m_0^2 t$. Then, it results

$$\begin{aligned} \langle m \rangle &= \frac{m_0(1 - \omega t)}{(1 + 2z)^{1/2}} + \frac{m_0 \omega t z}{(1 + 2z)^{3/2}} \\ &\quad - \epsilon\kappa m_0 t^2 \frac{3 + 4z + 2z^2}{(1 + 2z)^{5/2}} + \mathcal{O}(\epsilon^2, \epsilon\omega, \omega^2). \end{aligned} \quad (\text{A3})$$

Notice that the first two terms in the right-hand side come from the expansion of the deterministic Eq. (A2) up to first order in ω .

In particular, exactly at the critical point we have $\kappa = 1/3$ and $\lambda = 0$ (hence $\omega = \epsilon$). Therefore, as in the case of the OU approximation, one concludes that the magnetization remains $m \simeq m_0$ up to a characteristic time $\tau_0 \sim 1/\epsilon = N$.

Similarly, for $\langle m^2 \rangle$, one obtains the correction

$$C_2(\epsilon) = \epsilon t \sum_{k \geq 0} (k+1)(k+2)(-2z)^k = \frac{2\epsilon t}{(1+2z)^3},$$

leading to

$$\langle m^2 \rangle = \frac{m_0^2}{(1+2z)} - \frac{2\omega z(1+z)}{\kappa(1+2z)^2} + \frac{2\epsilon t}{(1+2z)^3} + \mathcal{O}(\epsilon^2, \epsilon\omega, \omega^2). \quad (\text{A4})$$

Since in the deterministic limit $\langle m^n \rangle = \langle m \rangle^n$, then the first two terms in the right-hand side come from the expansion of the squared Eq. (A2) up to first order in ω .

In the computation of the centered second moment, using Eqs. (A3) and (A4), the purely deterministic terms cancels out to yield Eq. (25).

Appendix B: Moment calculation near the spinodal

If $\epsilon = 0$, from Eq. (8) using $D_1 = -A(x^2 + 2A\alpha x - \alpha)$, $\alpha = \Delta h/(\beta J A)$ and $A \equiv \beta J m_{SP}$, the average magnetization is given by

$$\langle \Delta m \rangle = \sum_{k \geq 0} [-(x^2 + 2A\alpha x - \alpha) \partial_x]^k x (At)^k / k!, \quad (\text{B1})$$

where $x \equiv m_0 - m_{SP}$. Completing squares and making the change of variables $u = (x + A\alpha)/\sqrt{\gamma}$ with $\gamma = \alpha + A^2\alpha^2$ we obtain

$$\langle \Delta m \rangle = \sqrt{\gamma} \sum_{k \geq 0} [(1 - u^2) \partial_u]^k u (\sqrt{\gamma} At)^k / k! - A\alpha. \quad (\text{B2})$$

Considering the generating function for tangent, with the change of variable $u = \tanh z$, one has [14]

$$\begin{aligned} \sum_{n \geq 0} [(1 - u^2) \partial_u]^n u \tau^n / n! &= \sum_{n \geq 0} [\partial_z]^n \tanh z \tau^n / n! \\ &= (u + \tanh \tau) / (1 + u \tanh \tau), \end{aligned}$$

from where Eqs. (29)-(30) follow.

To include finite-size effects we have to consider the complete expression

$$\langle \Delta m \rangle = \sum_{k \geq 0} [D_1 \partial_x + D_2 \partial_{xx}]^k \frac{x t^k}{k!}. \quad (\text{B3})$$

When $\Delta h = 0$, from Eq. (27), we have $D_2(x) \simeq \epsilon(ax^2 + bx + c)$, with $a = \beta J - 2$, $b = -2m_{SP}$, $c = 1/\beta J$ and $D_1 = -Ax^2$. The contributions of order ϵ associated to each coefficient of the quadratic approximation of $D_2(x)$ are

$$\begin{aligned} C_{1a} &= -\frac{\epsilon a}{3A} \sum_{k \geq 2} (k^2 - 1)(-y)^k = -\frac{\epsilon a y^2 (3 + y)}{3A(1 + y)^3}, \\ C_{1b} &= \frac{\epsilon b t}{12} \sum_{k \geq 2} (k + 1)(3k - 2)(-y)^{k-1} = -\frac{\epsilon b t y (6 + 4y + y^2)}{6(1 + y)^3}, \\ C_{1c} &= -\epsilon c A t^2 \left(1 + \frac{1}{10} \sum_{k \geq 2} (k + 2)(2k + 1)(-y)^{k-1} \right) = -\frac{\epsilon c A t^2 (10 + 10y + 5y^2 + y^3)}{10(1 + y)^3}, \end{aligned}$$

where $y \equiv Axt$. Summing the ϵ -corrections $C_{1a} + C_{1b} + C_{1c}$ together with the deterministic one, given by Eq. (31), yields

$$\begin{aligned} \langle \Delta m \rangle &= \frac{x}{1 + y} - \left(\frac{c}{10Ax^2} (10 + 10y + 5y^2 + y^3) + \right. \\ &\quad \left. + \frac{b}{6Ax} (6 + 4y + y^2) + \frac{a}{3A} (3 + y) \right) \frac{\epsilon y^2}{(1 + y)^3}. \end{aligned} \quad (\text{B4})$$

Likewise, we calculate

$$\langle(\Delta m)^2\rangle = \sum_{k \geq 0} [D_1 \partial_x + D_2 \partial_{xx}]^k \frac{x^2 t^k}{k!}. \quad (\text{B5})$$

In this case, the contributions of order ϵ are

$$C_{2a} = -\frac{2ax}{A} \sum_{k \geq 1} \binom{k+2}{3} (-y)^k = \frac{2axy}{A(1+y)^4},$$

$$C_{2b} = -\frac{b}{12A} \sum_{k \geq 1} (k+1)(k+2)(3k+1)(-y)^k = \frac{by(12+6y+4y^2+y^3)}{6A(1+y)^4},$$

$$C_{2c} = ct \left(2 + \frac{1}{10} \sum_{k \geq 2} (k+1)(k+2)(2k+1)(-y)^{k-1} \right) = \frac{ct(10+10y+10y^2+5y^3+y^4)}{5(1+y)^4}.$$

Summing up the corrections $C_{2a} + C_{2b} + C_{2c}$, together with the deterministic term (given by the squared Eq. (31)), yields

$$\begin{aligned} \langle(\Delta m)^2\rangle &= \frac{x^2}{(1+y)^2} + \left(\frac{c}{5x}(10+10y+10y^2+5y^3+y^4) \right. \\ &\quad \left. + \frac{b}{6}(12+6y+4y^2+y^3) + 2ax \right) \frac{\epsilon y}{A(1+y)^4}. \end{aligned} \quad (\text{B6})$$

Finally, the second moment is obtained through $\Delta m^{(2)} = \langle(\Delta m)^2\rangle - (\langle\Delta m\rangle)^2$. The purely deterministic terms cancel out and at first order in ϵ it remains

$$\begin{aligned} \Delta m^{(2)} &= \frac{\epsilon y}{30Ax(1+y)^4} \left(20ax^2(3+3y+y^2) \right. \\ &\quad + 15bx(2+y)(2+2y+y^2) + \\ &\quad \left. + 12c(5+10y+10y^2+5y^3+y^4) \right) + \mathcal{O}(\epsilon^2). \end{aligned} \quad (\text{B7})$$

-
- [1] H.K. Janssen, B. Schaub, and B. Schmittmann, *Z. Phys. B - Condensed Matter* **73**, 539 (1989).
 - [2] V. V. Prudnikov, P. V. Prudnikov, I. A. Kalashnikov, and S. S. Tsirkin, *Journal of Experimental and Theoretical Physics* **106**, 1095 (2008).
 - [3] B. Zheng, *Int. J. Mod. Phys. B* **12**, 1419 (1998).
 - [4] B. Zheng, in *Computer Simulation Studies in Condensed Matter Physics*, edited by D. P. Landau, S. P. Lewis and H. B. Schüttler (Springer, New York, 2006).

- [5] V. V. Prudnikov, P. V. Prudnikov, A. S. Krinitsyn, A. N. Vakilov, E. A. Pospelov, and M. V. Rychkov, Phys. Rev. E **81** 011130 (2010).
- [6] E.S. Loscar, E.E. Ferrero, T.S. Grigera and S.A. Cannas, J. Chem. Phys. **131**, 024120 (2009).
- [7] W. Paul, D.W. Heermann and K. Binder, J. Phys A: Math. Gen. **22** 3325 (1989).
- [8] P. Hanggi, H. Grabert, P. Talkner and H. Thomas, Phys. Rev. A **29**, 371 (1994).
- [9] M. Munoz and P.L. Garrido, J. Phys A: Math. Gen. **28** 2637 (1995).
- [10] A. Pikovsky and S. Ruffo, Phys. Rev. E **59**, 1633 (1999).
- [11] F.T. Arecchi and A. Politi, Optics communications **29**, 362 (1979).
- [12] T. Mori, S. Miyashita and P.A. Rikvold, Phys. Rev. E **81**, 011135 (2009).
- [13] H. Risken, *The Fokker-Planck Equation: Methods of Solution and Applications* (Springer-Verlag, Berlin, 1984).
- [14] M.E. Hoffman, Electron. J. Combin. **6**, R21 (1999); D. Cvijović, Appl. Math. and Computation **215**, 3002 (2009).